

Physical and numerical modelling of the thermally induced wedging mechanism

C. PASTEN*, M. GARCÍA[†] and D. D. CORTES[‡]

Field observations and laboratory experiments show that temperature cycles can lead to wedging and accumulation of permanent displacements in several geosystems. The magnitude of these displacements depends on the geometric configuration of the components, the thermo-mechanical properties of the materials and interfaces, and the signature of the temperature signal. A physical model of a geometry susceptible to thermally induced wedging is analysed both experimentally and numerically in this article. The model consists of a driving wedge and a resisting block that rests on a rigid L-shaped base. The geometrical conditions required for the mechanism to manifest itself are found using equilibrium analysis of sliding and toppling. These conditions are reproduced in a physical model that is instrumented to measure changes in displacement and temperature in response to a cyclic temperature input. A numerical model was also developed to simulate the thermo-mechanical behaviour of the geometry. The numerical results and experimental measurements show that the accumulation of plastic displacement induced by temperature cycling is proportional to the period and amplitude of the input temperature signal.

KEYWORDS: finite-element modelling; model tests; repeated loading; temperature effects

ICE Publishing: all rights reserved

NOTATION

H	model height
L	model total length
L_B	block length
L_W	wedge length
T	thermal cycle period
β	wedge–block interface angle
δ_c	critical interface distance
η	base inclination angle
η_c	critical inclination value
μ	friction coefficient between block and base
μ_1	friction coefficient between wedge and base
μ_2	friction coefficient between wedge and block
φ	acrylic–aluminium friction angle

INTRODUCTION

Temperature changes and biased forces may cause accumulation of plastic displacement in geosystems consisting of discrete components and interfaces. Examples of thermally driven displacements have been recognised in natural rock slopes (Hatzor, 2003; Watson *et al.*, 2004; Gunzburger *et al.*, 2005; Vlcko *et al.*, 2009; Gischig *et al.*, 2011; Bakun-Mazor *et al.*, 2013), pavement structures (Croll, 2009), exposed geomembranes (Pasten & Santamarina, 2014a) and thermo-active piles (Pasten & Santamarina, 2014b).

One mechanism that explains accumulated displacements in jointed rock masses is thermally induced wedging, which involves the interaction of a driving wedge and a resisting block resting over a frictional surface that restrains its

movement. Changes in temperature induce volumetric changes in both elements and may trigger plastic displacements along the block–base and block–wedge interfaces (Bakun-Mazor *et al.*, 2013; Pasten, 2013; Greif *et al.*, 2014; Pasten *et al.*, 2015).

Experimental and numerical evidence that thermo-mechanical coupling can lead to wedging and ratcheting displacements has been presented previously (Pasten *et al.*, 2015). The study focused on deriving an analytical one-dimensional (1D) model that captures the parameter domain controlling the critical temperature required for the thermally induced wedging mechanism to manifest itself and corresponding numerical validation using the finite-element method.

The current article analyses the static stability against sliding and toppling of an idealised model and determines the main geometrical variables affecting the wedging mechanism. A physical model was built and tested to highlight the influence of the period and amplitude of the temperature cycles and numerical simulations were conducted to reproduce the experimental results. The thermally induced keyblock displacements reported by Bakun-Mazor *et al.* (2013) at Masada Mountain were then analysed to verify if the mechanism could be upscaled to realistic rock mass conditions.

THERMALLY INDUCED WEDGING MECHANISM

Model and mechanism description

In order to study the thermal wedging mechanism, a conceptual model that comprises a driving wedge and a resisting block lying on an orthogonal frictional base is analysed (Fig. 1(a)). The geometry of the model is defined by the total height H , the wedge length L_W , the block length L_B , the wedge–block interface angle β and the base inclination angle η . When the wedge expands, it reacts against the block and the base, resulting in the development of shear stress along the block–base interface. If the resulting displacement exceeds the critical displacement required to mobilise the

Manuscript received 22 May 2015; first decision 30 June 2015; accepted 24 July 2015.

Published online at www.geotechniqueletters.com on 21 August 2015.

*Department of Civil Engineering, University of Chile, Santiago, Chile

†Department of Geology, University of Chile, Santiago, Chile

‡Department of Civil Engineering, New Mexico State University, Las Cruces, NM, USA

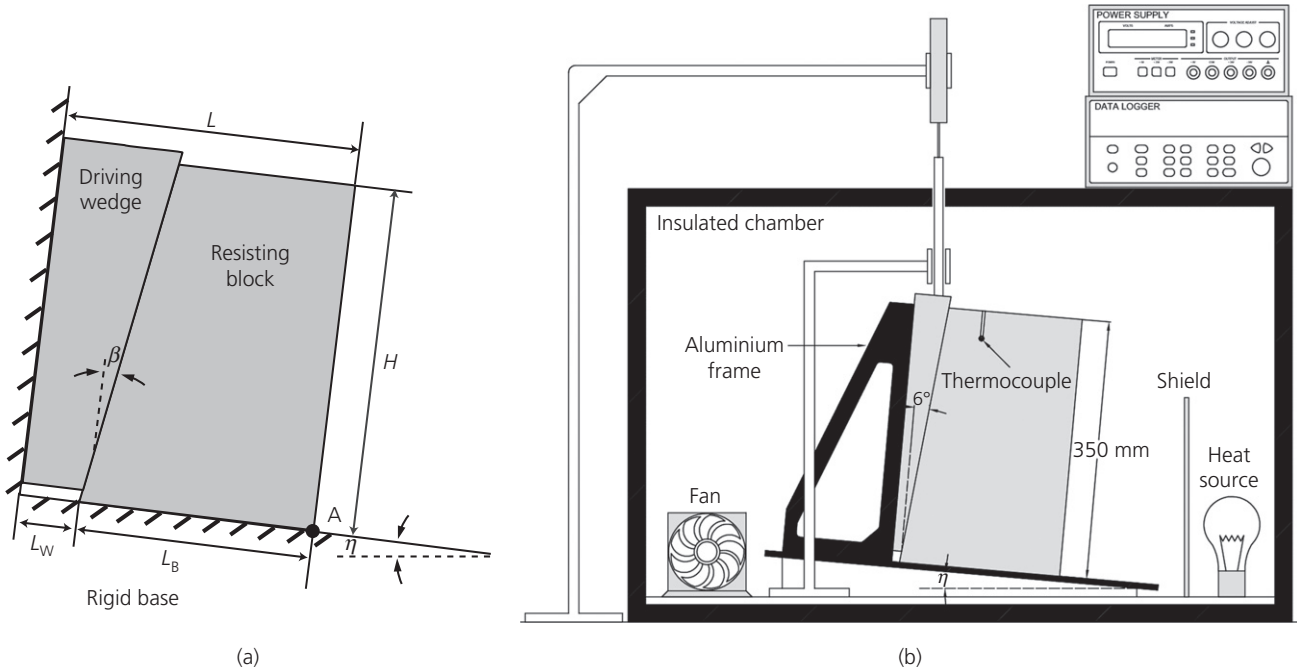


Fig. 1. Thermally induced wedging mechanism: (a) model configuration; (b) experimental setup

interface shear strength, the block experiences permanent displacement (Pasten *et al.*, 2015).

Static stability: sliding and toppling

Reduced stability can lead to sliding or toppling, both of which are different from – and incompatible with – the wedging mechanism. The stability of the system is verified considering normal and shear forces acting on the wedge and the block. The minimum relative block-to-wedge length ratio L_B/L_W that satisfies static stability of the wedge–block model (equation (1)) can be computed using equilibrium equations

$$\frac{L_B}{L_W} = \left[F(\mu, \mu_1, \mu_2, \beta, \eta) \cdot \left(1 - \frac{H}{2L_B} \tan \beta \right) - \frac{H}{2L_B} \tan \beta \right]^{-1} \tag{1}$$

where

$$F(\mu, \mu_1, \mu_2, \beta, \eta) = \frac{\mu - \tan \eta}{\mu_1 \tan \eta + 1} \cdot \frac{(\mu_1 + \mu_2) \left(\frac{\tan \eta \cdot \tan(\eta + \beta) + 1}{\tan \eta - \tan(\eta + \beta)} \right) + \mu_1 \mu_2 - 1}{(1 - \mu \mu_2) \left(\frac{\tan \eta \cdot \tan(\eta + \beta) + 1}{\tan \eta - \tan(\eta + \beta)} \right) + \mu + \mu_2}$$

and μ is the friction coefficient between the block and the base, μ_1 is the friction coefficient between the wedge and the base, and μ_2 is the friction coefficient between the wedge and the block.

Scaled physical models were tested and it was found that toppling depends on the total length $L = L_W + L_B$ (see Fig. 1(a)) and occurs when the critical inclination value η_c in equation (2) is exceeded. This observation is in agreement with the condition proposed by Goodman (1989) for a solid rectangular element.

$$\eta_c = \tan^{-1} \left(\frac{L}{H} \right) \tag{2}$$

In practice, toppling applies for very slender sliding-stable models with large L_B/L_W ratios. The critical value η_c corresponds to the inclination when the centre of gravity of the wedge–block system, which is almost identical to the block centre of gravity, moves to the right of point A (Fig. 1(a)). Although the friction between the driving wedge and the resisting block cannot usually sustain the wedge weight, simultaneous sliding of the small wedge does not prevent rotation with respect to point A and toppling is kinematically admissible

Equations (1) and (2) are used to determine the geometrical conditions that ensure static stability. Figure 2 shows the boundaries that delimitate the stable zones for different values of β and slenderness ratios H/L as a function of relative block-to-wedge length ratio L_B/L_W and η . The results in Fig. 2 show that

- models with low slenderness ratios, low interface angles β and large relative block-to-wedge length ratios L_B/L_W are more stable against toppling and sliding
- the toppling condition can be more restrictive than the sliding condition for models with high slenderness ratios and high L_B/L_W
- the destabilising effect of β is more pronounced in models with high slenderness ratios.

The analytical results are consistent with the observed increase in critical temperature required to trigger an accumulation of plastic displacements when the relative block-to-wedge length ratio L_B/L_W increases (Pasten *et al.*, 2015). Furthermore, it is expected that geometries at the verge of static equilibrium will be particularly susceptible to thermally induced wedging.

EXPERIMENTAL STUDY

Experimental setup: temperature-controlled chamber

A small-scale physical wedge model was built with a slenderness ratio $H/L = 1.5$. The model geometry is defined by length $L = 225$ mm, height $H = 350$ mm, $\beta = 6^\circ$ and $\eta = 0^\circ$, which ensures the model is inside the stable zone, as depicted by the red square in Fig. 2(e). The wedge and the block were

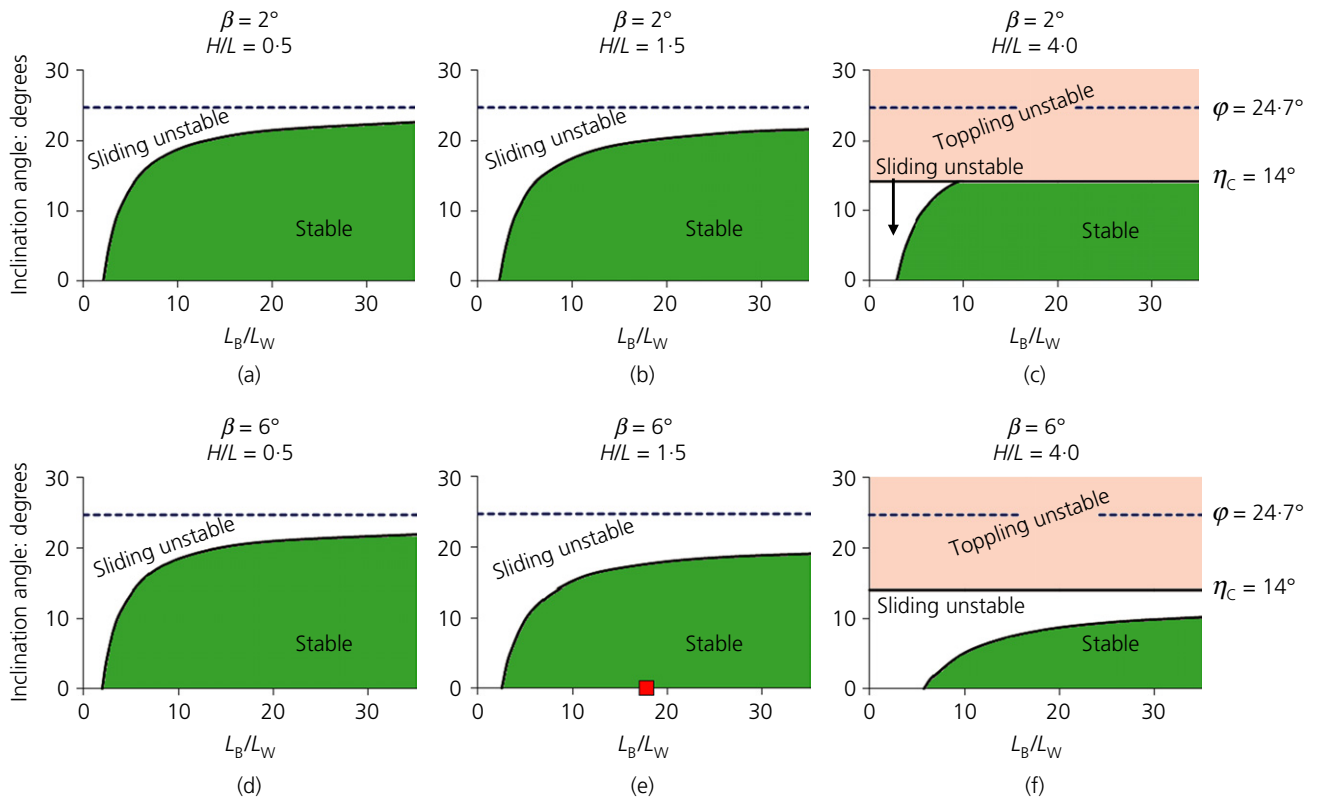


Fig. 2. Stability charts. The boundary of the green-shaded stable zone was calculated using equation (1). The area shaded in pink represents inclination angles for which the model is toppling unstable and the red square in (e) corresponds to the physical and numerical model analysed in Figs 3 and 4. The height in all cases was $H=350$ mm; $\eta_c=14^\circ$ is the critical angle for toppling for a slenderness ratio $H/L=4$ (evaluated with equation (2)); $\varphi=\text{atan } \mu$ is the friction angle of the interface between acrylic and aluminium ($\mu=\mu_1=0.46$) and the friction coefficient of the block–wedge interface is assumed equal to that of acrylic–acrylic $\mu_2=0.36$

manufactured from acrylic, and aluminium was used in the orthogonal base. The choice of materials provides a high thermal expansion contrast (material properties are listed in Table 1). The model components were placed inside a temperature-controlled chamber and instrumented with a linear variable differential transformer (LVDT) and thermocouples to monitor absolute vertical wedge displacements and temperature changes inside the block. Heat was provided via a light bulb using a refractive screen to eliminate direct-source radiation into the acrylic and aluminium elements (Fig. 1(b)). Temperature cycles were modulated by a thermostat.

The test comprised three stages. In the first stage, the model was heated until a constant offset temperature was reached. The second stage consisted of cycling the temperature at constant amplitude. Finally, the heat source was turned off, allowing the entire system to cool.

Experimental results

Temperature and vertical displacement measurements for a geometry with a base inclination $\eta=0^\circ$ are shown in Fig. 3. The induced cyclic temperature signals can be characterised as

- 65°C DC offset, 0.9°C peak-to-peak amplitude and 30 min period (Fig. 3(a))
- 63°C DC offset, 1.4°C peak-to-peak amplitude and 40 min period (Fig. 3(b))
- 66°C DC offset, 3.2°C peak-to-peak amplitude and 60 min period (Fig. 3(c)).

Initial heating causes thermal expansion and a positive vertical wedge displacement (wedge uplift). Later, thermal cycles induce an expansion–contraction sequence until the system is allowed to cool to the initial temperature and contracts, resulting in a sustained accumulation of negative

Table 1. Thermo-mechanical material properties

Parameter	Acrylic	Aluminium	Dolomite
Young's modulus, E : GPa	2.5	70	40
Mass density, ρ : kg/m^3	1180	2700	2600
Poisson's ratio, ν	0.4	0.3	0.2
Thermal expansion coefficient, α : $10^{-6}/^\circ\text{C}$	85	20	7
Thermal conductivity, k_T : (W/(m K))	0.2	210	1.7
Specific heat capacity, c_p : (J/(kg K))	1500	900	810
Thermal diffusivity, D_T : m^2/s	1.13×10^{-7}	8.64×10^{-5}	8.07×10^{-7}

Note: Measured interface friction coefficient between acrylic and acrylic is $\mu_2=0.36$ and the friction coefficient between acrylic and aluminium is $\mu=0.46$

vertical wedge displacement. The influence of temperature cycles on the vertical displacements depends upon the amplitude and period of the cycles. Only elastic displacements were observed as a result of the first induced cyclic temperature signal (Fig. 3(a)). In contrast, the second and third induced cyclic temperature signals resulted in the accumulation of vertical wedge displacement at a rate of 0.18 and 0.30 mm/cycle, respectively (Figs 3(b) and 3(c)).

NUMERICAL SIMULATIONS

Numerical model

A three-dimensional (3D) numerical model was developed using Abaqus 6.13 (Dassault Systèmes, 2013). Material thermo-mechanical properties, geometry and induced cyclic temperature signals were selected to reproduce the experimental conditions. Shear behaviour at the interfaces between the elements was modelled as elastic-perfectly plastic with a critical distance δ_c to mobilise the interface shear strength and a friction coefficient μ . In the absence of specific interface data, the critical distance adopted for all cases was $\delta_c = 1 \times 10^{-4}$ m. The interfaces were given a near-zero thermal conductivity value to prevent heat transfer across bodies. All bodies were modelled as elastic and discretised with C3D8T elements (four-node, full integration, coupled temperature-displacement elements). The metal base and acrylic block and wedge properties are listed in Table 1. Following the experimental models, a base inclination of $\eta = 0^\circ$ was used in all numerical simulations.

Temperature boundaries were imposed on all exposed surfaces to emulate the three thermal stages observed in the experiments. Boundary conditions were selected to match the measured temperatures inside the blocks. The input temperature signals consisted of

- 65°C DC offset, 4.0°C peak-to-peak amplitude and 30 min period
- 63°C DC offset, 5.6°C peak-to-peak amplitude and 40 min period
- 66°C DC offset, 6.4°C peak-to-peak amplitude and 60 min period.

Time increments were allowed to vary in order to improve convergence and to ensure that at least ten temperature increments were applied in every thermal cycle.

Numerical results

Numerical simulation results for temperature cycles with periods $T = 30, 40$ and 60 min are presented in Fig. 4. Similar to the experimental results, the 30 min period temperature signal caused elastic wedge displacements, whereas accumulated plastic displacement appeared for temperature signals with periods $T = 40$ min and $T = 60$ min. As in the physical tests, the combination of exposure time and temperature amplitude controlled the magnitude of accumulated displacement. The displacements per cycle obtained from the numerical tests (0.10 and 0.17 mm/cycle) compare reasonably well with the values measured in the physical tests (0.18 and 0.30 mm/cycle) for signals with periods $T = 40$ min and $T = 60$ min.

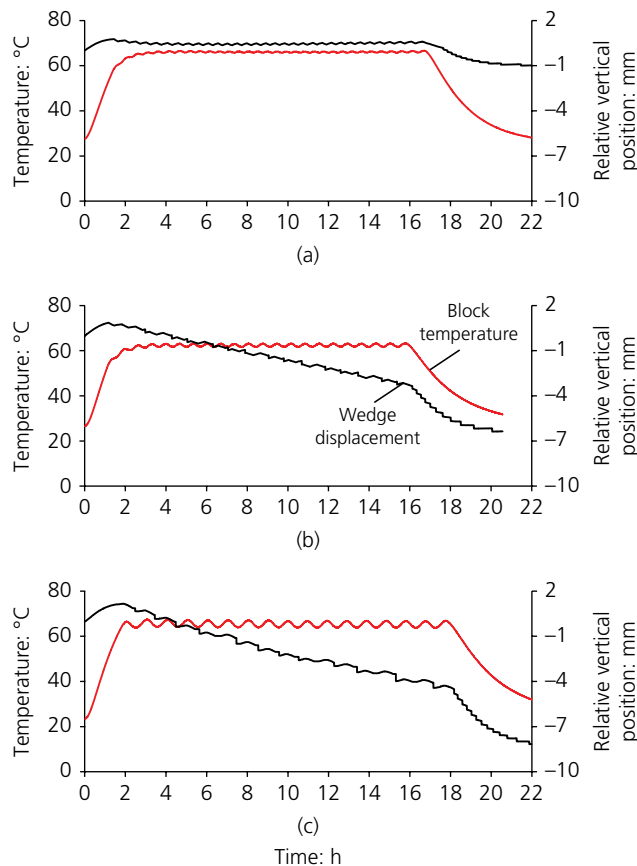


Fig. 3. Experimental results: (a) 30 min, (b) 40 min and (c) 60 min period temperature signals. The black lines show the wedge absolute vertical displacement and red lines show the temperature inside the block; $L_B = 213$ mm, $L_W = 12$ mm, $H = 350$ mm and $\beta = 6^\circ$

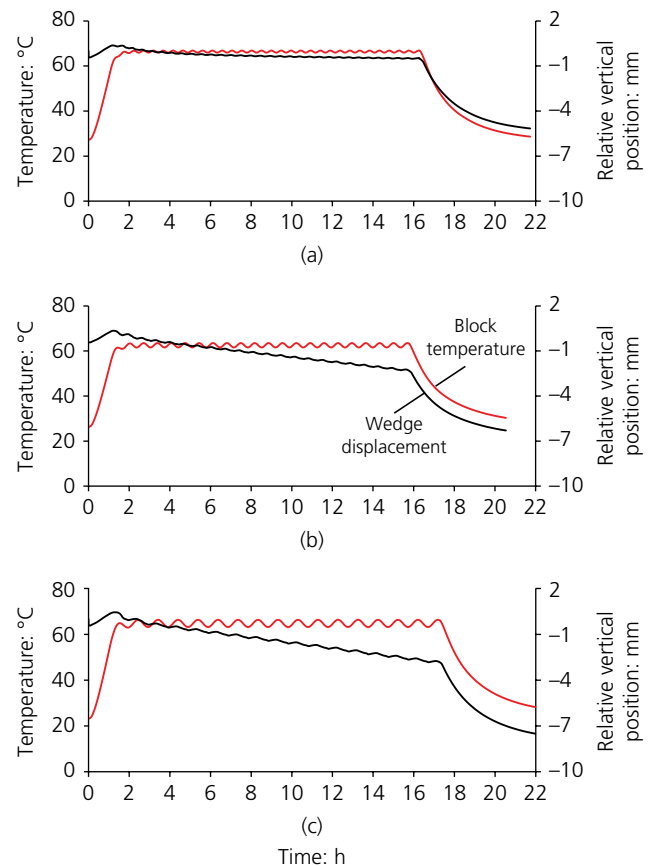


Fig. 4. Numerical results: (a) 30 min, (b) 40 min and (c) 60 min period temperature signals. The black lines show the wedge absolute vertical displacement and red lines show the temperature inside the block; $L_B = 213$ mm, $L_W = 12$ mm, $H = 350$ mm, $\beta = 6^\circ$, $\mu = \mu_1 = 0.46$ and $\mu_2 = 0.36$

EXAMPLE OF FIELD SITUATION

The developed numerical approach was slightly modified to study, under plane-strain conditions, the thermally induced keyblock displacements at Masada Mountain reported by Bakun-Mazor *et al.* (2013). The material thermo-mechanical properties adopted for dolomite rock are presented in Table 1 and the geometry of the system was considered as $H=15$ m, $L=8.4$ m, $L_w=0.9$ m, $\eta=19^\circ$ and $\beta=3^\circ$. In the absence of specific field data, a friction angle $\phi=28.7^\circ$ and a critical distance $\delta_c=2 \times 10^{-2}$ m were adopted for all the interfaces. The model geometry is sliding- and toppling-stable according to equations (1) and (2). At the edges of the wedge and the block, a sinusoidal temperature signature was imposed with an amplitude of 10°C and periods of half a day and half a year to represent daily and annual temperature fluctuations, respectively (Hatzor, 2003).

The limited thermal skin depth induced by a daily temperature fluctuation did not cause plastic block displacements. However, block plastic displacements accumulated at a rate of 0.5 mm/year in the base dip-direction when an annual temperature variation was applied. This value is of the same order of magnitude as the values measured by Hatzor (2003) and estimated by Bakun-Mazor *et al.* (2013). Even though these displacements are realistic, the solution is very sensitive to both the adopted critical distance δ_c and the friction angle. Additional analyses should be thus performed before a definite conclusion can be drawn.

DISCUSSION AND CONCLUSIONS

A conceptual model was proposed to capture thermally induced wedging, a mechanism very relevant to geosystems composed of discrete elements and interfaces subjected to biased forces and temperature cycles such as jointed rock masses. Conditions for sliding and toppling were identified. The results indicate that models with low slenderness ratios, low interface angles β and large relative block-to-wedge length ratios L_B/L_W are more stable against toppling and sliding. In addition, the toppling condition can be more restrictive than the sliding condition for models with high slenderness ratios and high L_B/L_W . The destabilising effect of β was more pronounced in models with high slenderness ratios. Models at the verge of static instability should be more susceptible to thermally induced wedging.

A simplified 3D numerical model composed of elastic materials and elastic–perfectly plastic interfaces was found to capture the mechanism. The numerical model could be used to extend the study and explore problems with more complicated geometries and/or boundary conditions. The numerical results obtained showed that the displacement accumulation is proportional to the combination of the amplitude and the period of the temperature cycle, which is consistent with experimental evidence from physical models.

The analysis of a keyblock at Masada Mountain in plane-strain conditions indicated that the wedging mechanism may be used to predict the accumulation of plastic displacement when a rock mass is subjected to relatively large annual temperature fluctuations.

ACKNOWLEDGEMENTS

Support for this research was provided by a Conicyt Fondecyt Initiation into Research grant (no. 11130363). Antonio Hernandez performed all the experimental tests.

REFERENCES

- Bakun-Mazor, D., Hatzor, Y. H., Glaser, S. D. & Carlos Santamarina, J. (2013). Thermally vs. seismically induced block displacements in Masada rock slopes. *Int. J. Rock Mech. Mining Sci.* **61**, 196–211.
- Croll, J. G. (2009). The role of thermal ratcheting in pavement failures. *Proc. Inst. Civ. Eng. Transport* **162**, No. 3, 127–140.
- Dassault Systèmes (2013). *Abaqus version 6.13*. Providence, RI: Dassault Systèmes.
- Gischig, V. S., Moore, J. R., Evans, K. F., Amann, F. & Loew, S. (2011). Thermomechanical forcing of deep rock slope deformation: 2. The Randa rock slope instability. *J. Geophys. Res. Earth Surf.* **116**, No. F4, F04011.
- Goodman, R. E. (1989). *Introduction to rock mechanics*. New York, NY: Wiley.
- Greif, V., Simkova, I. & Vlcko, J. (2014) Physical model of the mechanism for thermal wedging failure in rocks. In *Landslide science for a safer geoenvironment* (K. Sassa, P. Canuti & Y. Yin (eds)). Heidelberg: Springer, pp. 45–50.
- Gunzburger, Y., Merrien-Soukatchoff, V. & Guglielmi, Y. (2005). Influence of daily surface temperature fluctuations on rock slope stability: case study of the Rochers de Valabres slope (France). *Int. J. Rock Mech. Mining Sci.* **42**, No. 3, 331–349.
- Hatzor, Y. H. (2003). Keyblock stability in seismically active rock slopes – Snake Path Cliff, Masada. *J. Geotech. Geoenviron.* **129**, No. 8, 697–710.
- Pasten, C. (2013). *Geomaterials subjected to repetitive loading: implications on energy systems*. Atlanta, GA: Georgia Institute of Technology.
- Pasten, C. & Santamarina, J. C. (2014a). Experimental and numerical modeling of thermally-induced ratcheting displacement of geomembranes on slopes. *Geosynth. Int.* **21**, No. 6, 334–341.
- Pasten, C. & Santamarina, J. C. (2014b). Thermally induced long-term displacement of thermoactive piles. *J. Geotech. Geoenviron. Engng* **140**, No. 5, 06014003.
- Pasten, C., Garcia, M. & Santamarina, J. C. (2015). Thermo-mechanical ratcheting in jointed rock masses. *Geotech Lett.* **5**, April–June, 86–90.
- Vlcko, J., Greif, V., Grof, V. *et al.* (2009). Rock displacement and thermal expansion study at historic heritage sites in Slovakia. *Environ. Geol.*, **58**, No. 8, 1727–1740.
- Watson, A. D., Moore, D. P. & Stewart, T. W. (2004) Temperature influence on rock slope movements at Checkerboard Creek. *Proc. 9th Int. Symp. on Landslides, Rio de Janeiro, Brazil* **2**, pp. 1293–1298.

WHAT DO YOU THINK?

To discuss this paper, please email up to 500 words to the editor at journals@ice.org.uk. Your contribution will be forwarded to the author(s) for a reply and, if considered appropriate by the editorial panel, will be published as a discussion.